Journal of Materials Chemistry A

ROYAL SOCIETY OF CHEMISTRY

PAPER

View Article Online
View Journal

Cite this: DOI: 10.1039/d6ta00623j

Giant electrocaloric response in thiourea under a low electric field in the cryogenic region

Juan Manuel Bermúdez-García, †*[a] Susana Yáñez-Vilar, †[b] Angel Ferradanes-Martínez, [a] Antonio Luis Llamas-Saiz, [c] Manuel Sánchez-Andújar, [a] Socorro Castro-García, [a] María Antonia Señarís-Rodríguez [a] and Jorge Mira *[b]

Received 22nd January 2026
Accepted 26th March 2026

DOI: 10.1039/d6ta00623j

rsc.li/materials-a

In this work, almost 70 years after thiourea ferroelectricity was discovered, we report hitherto undiscovered electrocaloric properties in this compound. Remarkably, it exhibits a giant electrocaloric strength ($\Delta S/\Delta E$ = 1.13 J cm kg^{-1} kV^{-1}) and a large electrocaloric tunability (dT_t/dE = 0.7 K cm kV^{-1}), comparable to the best bulk electrocaloric materials reported to date, while requiring an exceptionally low electric field. Furthermore, we identify that electrocaloric effects can be further enhanced through the application of external pressure, making this material a new member of the emerging family of multicaloric materials. We relate such giant electrocaloric parameters to the large dielectric dipole, low molecular weight and weak chemical interactions, especially H-bonds, between the thiourea molecules of the crystal structure. Interestingly, these electrocaloric effects occur near 170 K, which could be useful for electrocaloric cooling to support liquid nitrogen cryogenic systems.

1. Introduction

In 1828, Friedrich Wöhler helped establish modern organic chemistry with the synthesis of urea (CH_4N_2O), the first organic compound directly obtained from an inorganic compound.[1] A few years later, Marceli Nencki obtained in his laboratory the analogue sulfur compound, thiourea (CH_4N_2S),[2] which was one of the earliest organic crystal structures to be studied[3] and was shown to exhibit ferroelectric properties.[4] Extensive studies on its unique ferroelectric behaviour have been performed since then.[5–11]

This compound exhibits multiple dielectric transitions associated with different solid–solid phase transitions. From the structural point of view, thiourea crystals present five different polymorphs depending on temperature. The low temperature phase I (T < 168 K) shows an orthorhombic symmetry with a non-centrosymmetric space group ($P2_1ma$), while the high temperature phase V (T > 202 K) exhibits an orthorhombic symmetry with a centrosymmetric space group ($Pnma$).[5] The intermediate phases II to IV are modulated phases traditionally described as arising from sinusoidal modulations of atomic displacement.[8] The original studies by Goldsmith and White demonstrated that phases I and III are ferroelectric, II and IV are antiferroelectric, and V is paraelectric.[5] Meanwhile, later studies revealed that the transition temperatures of the different structures can be shifted by applying an electric field.[6,11] Moreover, there are some – although scarce – studies on thiourea thermal properties,[6,12] showing that the largest thermal changes occur during the first transition between phases I and II, with values of 6.6 cal mol^{-1} (380 J kg^{-1}). On the basis of the reported ferroelectric and thermal properties, we anticipate that thiourea can present interesting electrocaloric effects, which have not been explored to date.

Electrocaloric materials are compounds that exhibit large thermal changes (isothermal entropy changes or adiabatic temperature changes) under the application and removal of an external electric field, generally associated with first-order ferroelectric transitions.[13] This family of functional materials is very interesting for heating and cooling applications and can be the basis for more efficient and eco-friendly refrigeration technologies.[14,15] Particularly, cryogenic refrigeration is becoming a growing challenge in our society. Emerging technologies such as wind generators using superconducting materials[16] and cryogenic sensors and instruments in the reactivated space race need temperatures of 150 K and below.[17] Technologies based on cryogenic liquids (especially liquid nitrogen) provide a relatively easy and economical way to reach such temperatures. However, these technologies suffer from leaks and fluid losses and – in some cases – they can lead to carbon emissions similar to diesel-driven vapour compression systems.[18] For these reasons, new cryogenic technologies, such

[a]CICA – Centro Interdisciplinar de Química e Bioloxía and Departamento de Química, Facultade de Ciencias, Universidade da Coruña, 15071 A Coruña, Spain. E-mail: j.bermudez@udc.es

[b]Departamento de Física Aplicada and Instituto de Materiais (iMATUS), Universidade de Santiago de Compostela, 15782, Santiago de Compostela, Spain. E-mail: jorge.mira@usc.es

[c]Research Infrastructures Area X-ray Unit, Universidade de Santiago de Compostela, 15782 Santiago de Compostela, Spain

† These authors contributed equally to this work.

as cryocoolers, are being explored as replacements and/or in combination with cryogenic fluids. In that regard, recent reports highlight that one of the potential applications for electrocaloric materials yet to be explored is cryogenic refrigeration, where examples of electrocaloric materials are very limited since most of them operate between 250 and 500 K.[19–22]

From the technological point of view, an important challenge concerns the operating electric field required to induce the thermal changes. While reported electrocalorics in bulk can show larger energy density, they also require very large electric fields to exhibit sufficient caloric effects. For that reason, over the last years most efforts have been devoted to developing thin films and multilayer electrocalorics, where the required electric field is dramatically reduced, but the active mass is limited by the thickness and number of deposited layers.[19–22]

Inspired by previous results, where we identified new stimuli-induced functional properties and caloric effects in both classic compounds, such as inorganic perovskites and intermetallic compounds,[23,24] and emerging materials, such as hybrid perovskites and metal–organic frameworks or MOFs,[25,26] we have intuited that the classic ferroelectric compound thiourea could present hitherto undiscovered electrocaloric effects in the bulk state, with a large response under an electric field in the cryogenic temperature range. In that case, it would be useful for potential cryogenic refrigeration.

Surprisingly, and as we will show, this material exhibits an electrocaloric effect very similar to that found in the best bulk electrocaloric materials and even larger in some cases.[19–22] Moreover, thiourea exhibits a giant electrocaloric strength (dS/dE) and a large tunability (dT_t/dE) due to its remarkably large sensitivity towards an electric field. In addition, we investigate the relationship between the electrocaloric properties and the crystal structure of this compound in order to identify the key aspects that make this material very sensitive to the electric field, an interesting aspect for the design of future electrocaloric materials.

2. Results and discussion

2.1. Variable-temperature differential scanning calorimetry and dielectric studies

We have performed variable-temperature differential scanning calorimetry (VT-DSC) to evaluate the latent heat related to the phase transitions of thiourea. To the best of our knowledge, most DSC studies on thiourea have focused on evaluating its specific heat capacity upon heating and/or monitoring the melting and thermal decomposition of thiourea coupled with thermogravimetric analysis (TGA).[12,27–30] These previous DSC studies under heating revealed that the most energetic thermal transition is observed at ~170 K, while the rest of the transitions show a significantly much lower energy and/or are difficult to observe by calorimetry.[6,30] For that reason, we focus our studies on the narrow vicinity of this particular transition. In that regard, Fig. 1 shows the most energetic phase transition, corresponding to the transition I–II. This structural change occurs at a transition temperature of T_h ~169.6 K on heating and T_c ~168.6 K on cooling. To our knowledge, these are the first DSC

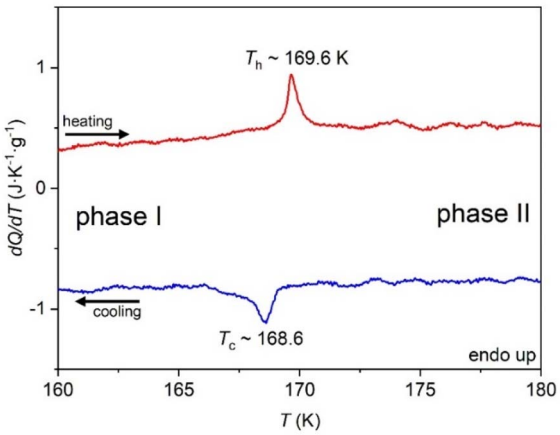

Fig. 1 Heat flow dQ/dT on cooling (blue) and heating (red) measured from 160 to 180 K at a rate of 1 K min^{-1}.

measurements to evaluate the reversibility of the phase transition upon heating and cooling.

Remarkably, our results show that the thermal hysteresis of this transition is very low with values of $(T_h–T_c)$ ~1.0 K, which is desired in caloric materials for reducing thermal losses associated with large thermal hysteresis.[31] Furthermore, the latent heat values of this transition are as large as ΔH ~340 J kg^{-1}, which is in agreement with the literature,[6] and more importantly is similar to the values observed for electrocaloric ceramics.[20]

In addition, we have also studied the temperature dependence of the real part of the relative permittivity along the polar a-axis as shown in Fig. 2. Here, we can observe anomalies of the real part of the relative permittivity related to the structural phase transitions between the different polymorphs (I, II, III, IV and V), in full agreement with literature data.[5]

The first dielectric transition from the ferroelectric (FE) phase I to the antiferroelectric (AFE) phase II starts at 168 K. The second transition between II (AFE) and III (FE) starts at 175 K.

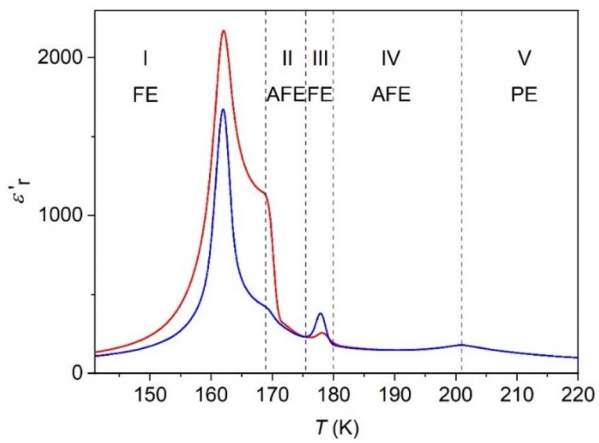

Fig. 2 Dielectric permittivity along the polar axis (ε_r') *versus* temperature (T) on cooling (blue) and heating (red) at $\nu = 1$ MHz. Note: regions I to V have been assigned according to ref. 5, 6 and 8.

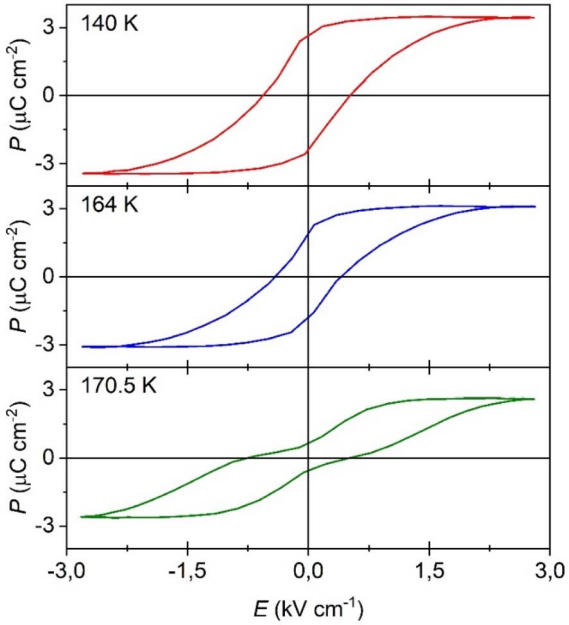

Fig. 3 Selected polarization loops below (140 K and 164 K) and above the transition temperature T_1 at $\nu = 927$ mHz.

The third transition between III (FE) and IV (AFE) commences at 180 K, and the last transition towards the paraelectric (PE) polymorph V occurs at 202 K. These transitions have been assigned following the literature.[5,6]

2.2. Electrocaloric effects in thiourea

From now on, for the study of caloric effects, we will focus on the first phase transition I–II due to its larger latent heat.

Below T_1 ~168 K, the polymorph I is ferroelectric and for 168 < T(K) < 175 the polymorph II is antiferroelectric, as observed from the polarization loops in Fig. 3, which is in agreement with the literature.[5]

The FE phase exhibits a saturation polarization value of P_s ~3.5 μC cm^{-2} under the application of electric fields as small as 3 kV cm^{-1}. When undergoing the phase transition, thiourea exhibits a double polarization loop characteristic of antiferroelectric materials. Those loops exhibit a saturation polarization of P_s ~2.6 μC cm^{-2} when increasing the electric field up to 3 kV cm^{-1}.

These values of polarization agree with values obtained by the integration of the pyroelectric effect related to the FE-AFE transition with a P_s ~2.7 μC cm^{-2} (see Fig. 4).

From the analysis of the polarization loops (Fig. S1 of the SI), we calculate the polarization change as a function of temperature for different applied electric fields (Fig. 5).

Further analysis of these curves allows us to make a first indirect estimate of the isothermal entropy change, ΔS, using the Maxwell eqn (1), which is a commonly used method to evaluate electrocaloric effects in ferroelectric materials:[13,32–34]

$$\Delta S = -\frac{1}{\rho}\int_{E_1}^{E_2}\left(\frac{\partial P}{\partial T}\right)\mathrm{d}E; \quad (1)$$

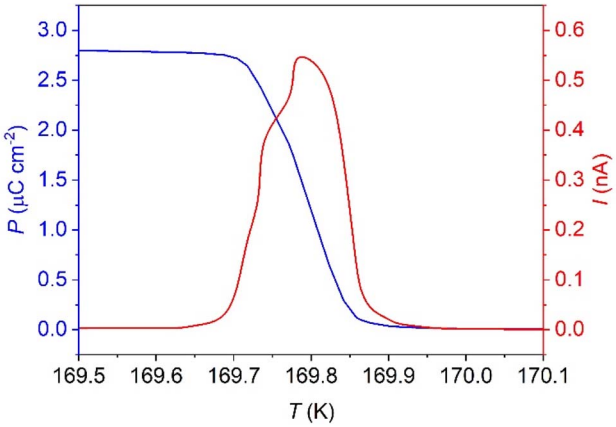

Fig. 4 Temperature dependence of the spontaneous polarization (blue curve) obtained by integrating the pyroelectric current (red curve).

where ρ is the density of the material.

As can be observed in Fig. 5, the isothermal entropy change increases up to 1.7 J K^{-1} kg^{-1} when applying an electric field as small as 1.5 kV cm^{-1}, resulting in a large electrocaloric strength of 1.13 J cm K^{-1} kg^{-1} kV^{-1}. This value is similar (and in some cases larger) than those shown by the best bulk electrocaloric materials reported to date.[32,35–41]

According to the polarization *versus* temperature curves (Fig. 5), which we have measured in the presence of different electric fields, the transition temperature shifts towards larger values when increasing the applied electric field with a dependency of dT_t/dE ~0.7 K cm kV^{-1}, which is in agreement with data obtained from the *E*–*T* phase diagram by Futama in the I–II limiting region (dT_t/dE ~0.9 K cm kV^{-1}).[6] This very large displacement together with the very small thermal hysteresis observed in our VT-DSC studies suggests that the electrocaloric effects – here calculated as ΔS ~1.7 J K^{-1} kg^{-1} using the

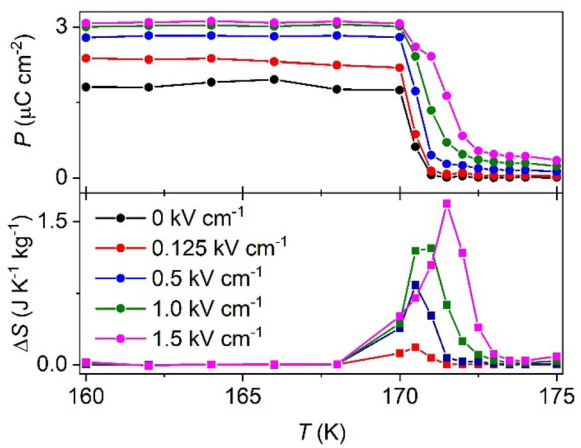

Fig. 5 Polarization change (top) and isothermal entropy change (bottom) as a function of temperature at different applied external electric fields.

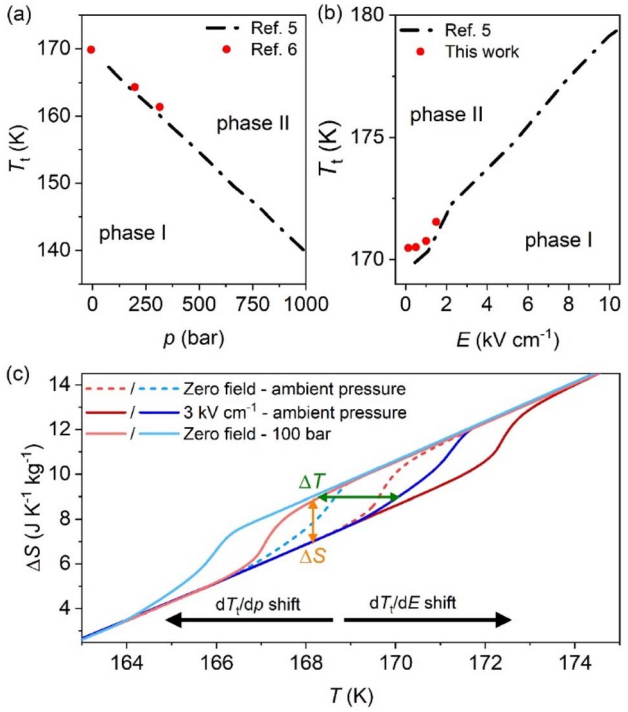

Fig. 6 (a) Transition temperature dependence with pressure (dT_t/dp). (b) Transition temperature dependence with applied electric field (dT_t/dE). (c) Isothermal entropy change curves (ΔS) under different conditions: (i) at zero applied field and ambient pressure (dashed lines), (ii) under the application of 3 kV cm^{-1} at ambient pressure, and (iii) under zero field at 100 bar. Note: heating curves are in red and cooling curves are in blue. Reversible values of ΔS and ΔT in orange and green arrows.

polarization curves – could be reversibly driven already under low applied electric fields.

For a deeper assessment of the electrocaloric effects, we have built VT-DSC curves using our experimental data, together with the E–T phase diagram reported in the literature.[6,7]

Furthermore, we have used the same strategy, considering reported p–T phase diagrams[6] for evaluating the barocaloric behavior induced by applied pressure on thiourea.

Fig. 6 shows the I–II transition temperature shift when applying pressure (panel a) and when applying an electric field (panel b). According to these data, we found that thiourea displays an inverse barocaloric coefficient of dT_t/dp = −29.7 K kbar^{-1}, ranking among the largest barocaloric coefficients reported to date.[42]

In the same line, Fig. 6c shows the isothermal entropy change curves (ΔS) of the sample under different conditions: (i) at zero applied field and ambient pressure (dashed lines), (ii) under the application of 3 kV cm^{-1} at ambient pressure, and (iii) under zero field at 100 bar (a pressure easily accessible by commercial compressors, especially in those of CO_2-based refrigeration systems).

These curves have been built considering the specific heat capacity C_p of thiourea[30] and our VT-DSC curves shifted according to the reported values of (dT_t/dp)[6,7] and (dT_t/dE).[6] This approach is a common practice in classic caloric studies, especially when very complex equipment would be required (*i.e.* calorimeter coupled to an electric field and high pressure in this case).[43–45]

Under these assumptions, the isothermal entropy changes can be obtained using eqn (2) as reported elsewhere:[13]

$$\Delta S = \int_{T_1}^{T_2} \frac{1}{T}\left(C_p(T, p_{atm}) + \frac{dQ}{dT}(T, i)\right) dT. \quad (2)$$

where T_1 and T_2 indicate the arbitrary initial and final temperature, i represents the electric field (or pressure) for each |dQ/dT| curve, and C_p is the heat capacity of the material for each temperature at atmospheric pressure (p_{atm}), which is considered independent of the applied pressure.

From these curves, we can extract several important conclusions regarding the caloric effects of thiourea: (i) thiourea can present inverse barocaloric effects, where the transition temperature shifts towards higher temperatures when increasing pressure; (ii) thiourea presents conventional electrocaloric effects, where the transition temperature shifts towards higher temperatures when increasing the applied electric field; (iii) we can combine an electric field and pressure to increase the caloric effects of thiourea, obtaining pressure-assisted electrocaloric effects or multicaloric effects.

In the latter aspect, in Fig. 6c, it can be observed that modulating the external conditions from zero field at 100 bar to 3 kV cm^{-1} at ambient pressure yields reversible caloric effects of ΔS ~1.9 J K^{-1} kg^{-1} (orange arrow in Fig. 6c) and ΔT ~1.8 K (green arrow in Fig. 6c). It should be noted that these values (particularly ΔS values) are in agreement with our previous calculations using the polarization curves under 1.5 kV cm^{-1}.

Even more remarkably, according to curves in Fig. 6, the caloric effects are already reversible under the application of a noticeably low electric field, only 3 kV cm^{-1}, and/or 100 bar, while most electrocaloric materials require electric fields of 10–1200 kV cm^{-1} (ref. 20, 21, 32, 35–41 and 46) and most barocaloric materials require pressures above 1000 bar.[42] The significant reduction of the required electric field and pressure open the door to designing safer devices with lower energy consumption and lower complexity.

Moreover, in order to further confirm the magnitude of the caloric effects, we also study the volume change across the phase transition (Fig. S2 of the SI) using single crystal X-ray diffraction, as further discussed in the following section. From this data, we can calculate the isothermal entropy change of the I → II phase transition related to the caloric effect using the Clausius–Clapeyron eqn (3):

$$\Delta S = \frac{\Delta v}{(dT_t/dp)} \quad (3)$$

where Δv is the specific volume change across the transition and dT_t/dp is the barocaloric coefficient. Following this additional method, we confirm that the isothermal entropy change shows a value of $\Delta S \sim 1.5$ J K^{-1} kg^{-1}, which is in agreement with the value calculated using the Maxwell equation (ΔS ~1.7 J K^{-1} kg^{-1}) and the value calculated from the constructed isothermal entropy change curves in Fig. 6 and eqn (2) (ΔS ~1.9 J K^{-1} kg^{-1}). Moreover, the specific volume change as a function of

Table 1 Caloric parameters of the best bulk electrocaloric materials reported to date. T_h is the transition temperature on heating, T_h-T_c is the thermal hysteresis, $|\Delta S|$ is the electrocaloric effect in terms of isothermal entropy change, $|\Delta E|$ is the externally applied electric field, $|\Delta S/\Delta E|$ is the electrocaloric strength in terms of entropy change, and $|dT_t/dE|$ is the electrocaloric tunability

Material (bulk)	Sample type	T_h (K)	T_h-T_c (K)	$\|\Delta S\|$ (J K^{-1} kg^{-1})	$\|\Delta E\|$ (kV cm^{-1})	$\|\Delta S/\Delta E\|$ (J cm K^{-1} kg^{-1} kV^{-1})	$\|dT_t/dE\|$ (K cm kV^{-1})	Ref.
Thiourea	Single crystal	170	1.0	1.7	1.5	1.13	0.7	This work
$(NH_4)_2SO_4$	Single crystals	224	2.8	19.0	11.0	1.72	5×10^{-3}	48
$RbHSO_4$	Single crystal	265	—	0.04	1.5	0.03	—	47
NH_4HSeO_4	Single crystal	250	0.7	0.1	1.35	0.07	1.6	49
$iBA_2EA_2Pb_3I_{10}$	Single crystal	~317	~6.0	33.3	18	1.85	—	34
iBA_2PbCl_4	Single crystal	302	10	25.6	29.7	0.86	—	33
$[(CH_3)_3NCH_2Cl]CdCl_3$	Single crystal	400	3.2	33.1	73	0.5	3.6×10^{-2}	50
(3-Pyrrolinium)$CdBr_3$	Single crystal	238	2.7	1.2	7.4	0.16	—	32
[MDABCO]$(NH_4)I_3$	Single crystal	448	54.0	36.0	20.0	1.8	0.11	35
KH_2PO_4	Single crystal	123	—	3.5	10	0.35	—	36
$BaTiO_3$	Single crystal	404	2.0	2.1	4.0	0.5	0.33	37
$Pb(Mg_{1/3}Nb_{2/3})_{0.75}Ti_{0.25}O_3$	Single crystal	383	—	—	25.0	—	—	38
$Pb_{0.99}Nb_{0.02}(Zr_{0.75}Sn_{0.20}Ti_{0.05})O_3$	Single crystal	434	—	—	30.0	—	—	39
$BaZr_{0.2}Ti_{0.8}O_3$	Ceramic	311	—	1.9	21.0	0.09	—	40
P(VDF-TrFE-CFE)	Polymer	303	—	73.5	1500.0	0.05	—	41

temperature (Fig. S2 of the SI) reveals that the transition temperature of the phase transition I→II takes place at T_t ~172 K, which is in full agreement with the T_t values obtained from our variable-temperature DSC (Fig. 1) and polarization data (Fig. 5), as well as with the dielectric regions previously identified by Godschmith and White (Fig. 2).[5,6,8]

When analysing the caloric parameters, thiourea exhibits a large electrocaloric strength ($\Delta S/\Delta E$ = 1.13 J cm kg^{-1} kV^{-1}) and electrocaloric tunability (dT_t/dE = 0.7 K cm kV^{-1}), which surpass the values of state-of-the-art bulk electrocaloric materials, such as the inorganic perovskite $BaTiO_3$ ($\Delta S/\Delta E$ = 0.5 J cm kg^{-1} kV^{-1}, dT_t/dE = 0.33 K cm kV^{-1})[37] and the metal-free perovskite MDABCO$(NH_4)I_3$ ($\Delta S/\Delta E$ = 1.8 J cm kg^{-1} kV^{-1}, dT_t/dE = 0.11 K cm kV^{-1})[35] (see Table 1).

Furthermore, thiourea exhibits electrocaloric effects in the cryogenic temperature (~170 K) region, where the only example is the molecular compound KH_2PO_4, while most reported electrocalorics operate near room temperature (250–500 K) (see Fig. 7).

2.3. Structural origin of the electrocaloric parameters

Most of the reported electrocaloric materials (including $BaTiO_3$ and MDABCO$(NH_4)I_3$) present an extended non-molecular structure, where the atoms are bonded by strong chemical interactions (such as covalent and ionic bonds). Meanwhile, thiourea (similarly to KH_2PO_4) is a molecular compound, where the bonding between the molecules is mainly based on weaker intermolecular interactions, namely hydrogen bonds. Additionally, the thiourea molecule is a low-molecular-weight polar species with a large electrical dipole of ~9 D[26] along the carbon–sulfur axis due to its planar conformation. Therefore, in comparison with large-molecular-weight species that are linked through stronger bonds, thiourea would require smaller electric fields to orient the electric dipoles and induce a phase transition, while allowing for the transition to occur at much lower temperatures.

In the literature, it is possible to find different data sets for the crystal structures of thiourea that have been generated since the 1930s. As these data have been compiled by different authors using different temperature ranges, different crystals and different instruments that have advanced over the years, some contradictions in the data are almost inevitable.[8,51–56]

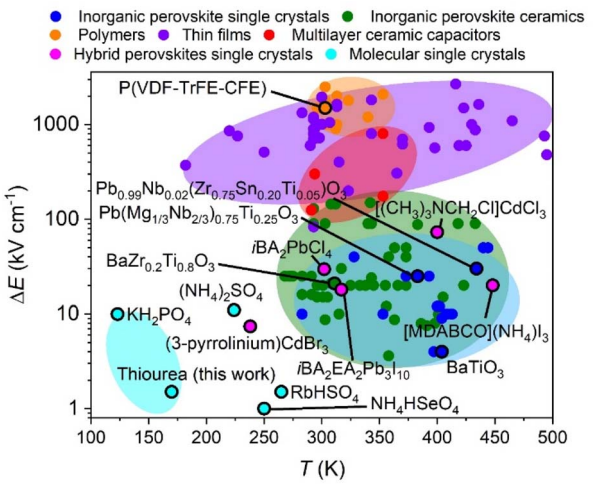

Fig. 7 Comparison of different families of electrocaloric materials in terms of the required electric field ΔE (kV cm^{-1}) for a given operating temperature T(K), where thiourea requires a much lower electric field to show electrocaloric effects while being one of the very few examples to operate in the cryogenic region. Data compiled from ref. 20, 21, 32–41 and 46–50. Note: selected bulk electrocalorics from Table 1 are highlighted. iBA = isobutylammonium; EA = ethylammonium; DABCO = 1,4 diazabicyclo[2.2.2]octane; P(VDF-TrFE-CFE) = poly(vinylidene fluoride-trifluoroethylene-chlorofluoroethylene).

In this work, and for the first time, we have been able to determine the crystal structures of the low-temperature and high-temperature polymorphs I and V, as well as an averaged crystal structure for the modulated phases related to II, III and IV phase regions, using the same crystal sample and a "state of the art" single crystal diffractometer. In this way, we have obtained a set of coherent and homogeneous results, which can serve as a basis for establishing structure–electrocaloric property relationships.

According to our single crystal X-ray diffraction structure determination, at $T \leq 172$ K, thiourea exhibits an orthorhombic phase I with the space group $P2_1ma$ (non-centrosymmetric). Meanwhile, at $T \geq 202$ K, phase V presents an orthorhombic symmetry with the centrosymmetric space group *Pnma*. Additionally, phases II to IV (modulated phases) also exhibit an orthorhombic symmetry with the centrosymmetric space group *Pnma* for the "average" structure refined using only the main reflections and not the satellite peaks. The raw collected and processed data considering the modulation and satellite peak integration are also available in an open access repository (see the Methods section).

The modulation vector describes the small structural changes that "break" the centrosymmetry allowing for the observed physical properties, like FE and AFE, which would otherwise be forbidden. For the refined modulated phases, even if we have not taken the modulation peaks into account, we obtain good agreement factors between the proposed model and the experimental data.

In all the crystal structures studied from 100 to 250 K, thiourea molecules are packed forming chains along the *b*-axis, where neighboring molecules are alternatively rotated ~180° and slightly shifted out of the plane of the chains (see Fig. 8 and S3 of the SI). Thiourea molecules are linked by H-bonds formed between the nitrogen and the sulfur (N–H···S). We observe two different types of H-bonds: the first ones are shorter and occur within the same chains (intrachain H-bonds), and the second ones are longer and occur between neighboring chains (interchain H-bonds) (see Fig. S4 of the SI).

Remarkably, we find that H-bonds play an important role in the observed phase transitions and dielectric response, as postulated in previous studies[56,57] and further detailed below.

The high-temperature phase V exhibits an asymmetric unit, which comprises half a sulphur atom, half a carbon atom, one nitrogen atom and two hydrogen atoms with the first two atoms located over the crystallographic mirror plane. Here, thiourea molecules along the same chain are ordered in an antiparallel arrangement related by crystallographic symmetry centers where the dipoles cancel out.

In the whole temperature range studied, we observe that the intramolecular bond lengths and angles of thiourea molecules are almost temperature independent. However, the disposition of the H-atoms and the relative orientations of thiourea molecules change with temperature.[56,57] We suggest that these distortions are provoked by changes in the H-bond strength as a function of temperature.

In this context, when the temperature lies between 168 K and 202 K (in the low-temperature phase and modulated phase regions), the H-atoms deviate from a coplanar arrangement. Meanwhile, when the temperature increases above 202 K, the H-atoms adopt a coplanar arrangement.

It should be noted that the 2 crystallographically independent H-atoms exhibit slightly different out-of-plane displacement values (Table S2 of the SI), but both are perfectly correlated.

As can be seen in Fig. S5 of the SI, we find that these displacements increase at lower temperatures with a maximum value at T ~176 K, which coincides with a maximum of the real part of the relative permittivity related to FE phase III. Therefore, the displacement of the H-atoms, which is likely induced by the strengthening of H-bonds at lower temperatures, seems to be responsible for the modulation of the crystal structures and for the dielectric transitions.

Below T ~176 K, the H-atom displacement decreases, inducing a new distortion of the crystal structure related to the AFE to FE phase transition from polymorph II to I. As a consequence, in the low temperature phase I, two types of thiourea

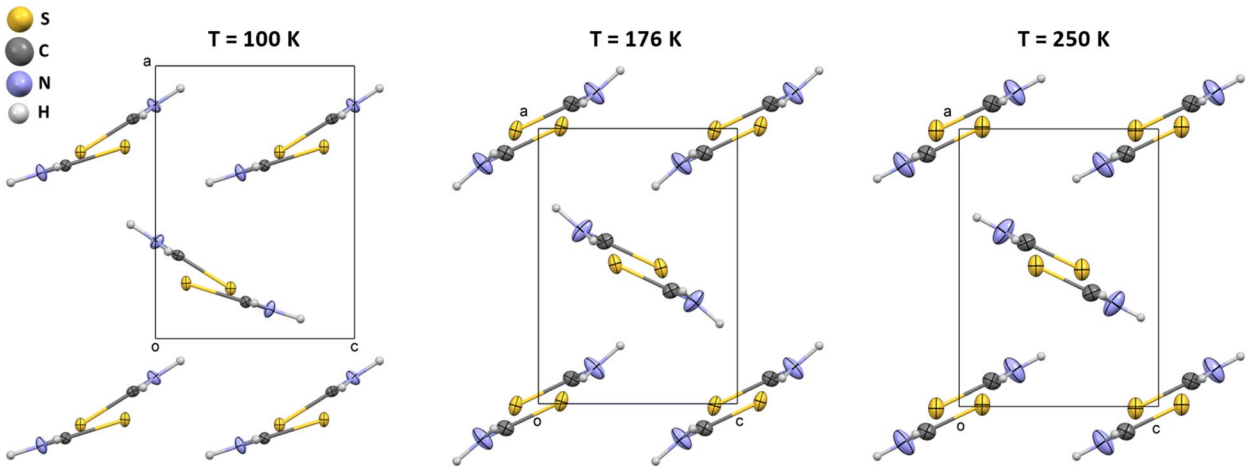

Fig. 8 Crystal structures obtained by single-crystal X-ray diffraction at T = 250 K, 176 K and 100 K.

molecules appear, which are no longer in a centrosymmetric arrangement, unlike in phase V. In phase I, both types of thiourea molecules are slightly tilted breaking the anti-parallel arrangement and resulting in the appearance of a net polarization along the *a*-axis. From the crystallographic point of view, this tilting is described by the irreducible representation ($GM3^-$) of the parent space group *Pnma*, where the associated order parameter corresponds to the magnitudes of the tilting between neighbouring thiourea molecules.

In summary, we find that the H-bonds might be the driving force behind the structural and dielectric transitions in the thiourea crystals. The strength of this intermolecular interaction is strongly temperature dependent, which gives rise to the temperature-induced multiple transitions, including the AFE to FE transition responsible for the large electrocaloric effect. In addition, the relative weakness of these interactions allows an easy reorientation of the thiourea dipoles under an applied electric field, leading to the remarkably giant electrocaloric strength tunability found in this compound.

3. Conclusions

In this work, we report for the first time the electrocaloric effects of a classic organic compound that was one of the earliest and most intensively studied crystal structures and ferroelectric materials reported in the literature, thiourea.

Remarkably, this organic compound is one of the few examples of electrocaloric materials that can operate in the cryogenic temperature range, a temperature regime that has recently attracted the interest of the scientific community working on electrocaloric materials and technologies. Furthermore, thiourea exhibits a significantly large electrocaloric strength ($\Delta S/\Delta E = 1.13$ J cm kg^{-1} kV^{-1}) and electrocaloric tunability ($dT_t/dE = 0.7$ K cm kV^{-1}), which surpass the values of state-of-the-art bulk electrocaloric materials, attributed to the significantly low operating electric field of only [1.5–3.0] kV cm^{-1}. Even more interestingly, we have identified that the ferroic transition responsible for the electrocaloric effect can be modulated with pressure, so thiourea can present enhanced pressure-assisted electrocaloric effects. By combining applied pressure and an electric field, thiourea can present caloric effects of $\Delta S \sim 1.9$ J K^{-1} kg^{-1} and $\Delta T \sim 1.8$ K, making this compound a new example of the emerging class of multicaloric materials.

In addition, we have also investigated the relationships between the structure and the electrocaloric effect identifying key aspects that allow us to clarify the origin of this outstanding behavior and give clues to design enhanced electrocaloric materials in the future. In this case, we find that the molecular nature of this compound with a low molecular weight, an associated large electric dipole and weak chemical interactions between molecules, mainly H-bonds, is responsible for its large electrocaloric response and allow for structural transitions to occur at lower temperatures than in most electrocaloric materials. These findings open the door to future studies on molecular electrocaloric materials with enhanced strengths and tunability.

4. Methods

4.1. Crystal preparation

Single crystals of thiourea (Fig. S6 of the SI) were grown using a method reported elsewhere.[5] For this purpose, a saturated methanol solution of thiourea (Sigma-Aldrich ≥99.0%) was maintained undisturbed to allow for evaporation under open air conditions. After a few weeks, transparent millimeter-sized and hexagonal-plate shaped single crystals were obtained.

4.2. Single crystal X-ray diffraction

Single-crystal X-ray diffraction experiments were carried out at different temperatures, spanning all the phase transitions from below to above. For this purpose, 17 single-crystal diffraction data sets of one crystal were collected at different temperatures between 100 and 250 K using a Bruker D8 VENTURE Kappa X-ray diffractometer equipped with a PHOTON III detector under monochromatic MoKα radiation ($\lambda = 0.71073$ Å).

A suitable crystal was chosen and mounted on a MiTeGen MicroMount™ using Paratone® N (Hampton Research). The temperature of the crystal was changed at a 200 K hour^{-1} rate, blowing the sample with a stream of nitrogen gas from an Oxford Cryosystem 800 Plus cooler. The data integration and reduction were performed using the APEX3 v2019.1-0 (ref. 58) software suite. The integrations of the reflections were performed with SAINT 8.38A and the intensities collected were corrected for Lorentz and polarization effects and for absorption by semi-empirical methods based on symmetry-equivalent data using SADABS 2016/2 of the APEX3 suite software. The structures were solved using the dual-space algorithm implemented in the SHELXT2018/2 program (ref. 59) and were refined by the least squares method using SHELXL2018/3.[60]

Detailed experimental crystallographic data for thiourea at $T = 100$, 130, 150, 160, 165, 170, 172, 174, 176, 178, 180, 185, 190, 200, 202, 210, and 250 K are included in Table S1 of the SI. CCDC 2039156–2039172 contains the supplementary crystallographic data for this paper. Full raw diffraction datasets for the 17 measured temperatures are hosted and completely available on Zenodo (https://zenodo.org/communities/thiourea) to ensure reproducibility and long-term data preservation.

4.3. Dielectric and ferroelectric properties

The real (ε') and imaginary (ε'') parts of the dielectric permittivity were measured using a Precision LCR Meter (HP 4284 A) in the frequency range 10^2–10^6 Hz and using a voltage of 0.1 V. For this purpose, we deposited gold electrodes (area ~0.14 mm^2) on a crystal oriented along the polar axis (length ~2 mm). The temperature was controlled using a He closed cycle cryogenic system (Displex ADP-Cryostat HC-2), equipped with a digital temperature controller (IEE-488 Status). The temperature range measured varied from 10 K to 300 K with a rate of 1 K min^{-1}. In addition, we registered the Cole–Cole diagrams between 160 K and 170 K.

The ferroelectric hysteresis loops (*P*–*E*) were traced using a modified Sawyer-Tower[17] circuit with a sinusoidal signal at a frequency of 927 mHz.

4.4. Pyroelectric properties

The pyroelectric behavior was examined with a direct method, in which the charge released with a given incremental temperature change as a function of temperature was measured with a Keithley 617 electrometer. For this purpose, gold electrodes (area ~0.14 mm^2) were sputtered on opposite sides of a single crystal (length ~2 mm). The sample was first cooled in an electric field (50 V) from 190 K to 140 K (rate 1 K min^{-1}); then, the electric field was removed and the $I(T)$ curve was recorded during heating and cooling at a temperature sweep rate of 1 K min^{-1}. Before heating from 140 to 190 K and cooling from 190 K to 140 K, a time dependence of electric charge was recorded for 1800 s to ensure stability. The polarization was calculated following eqn (4) as reported elsewhere:[61]

$$P = \frac{1}{rA}\int_{T_1}^{T_2} I\,dT \quad (4)$$

where r is the heating/cooling rate, A is the electrode area, and I is the pyroelectric current.

4.5. Differential scanning calorimetry

Differential scanning calorimetry was carried out using a Setaram Setline DSC in the range of 130–180 K with a heating/cooling ramp of 1 K min^{-1}, using ~4 mg of sample. For indirect assessment of electrocaloric and barocaloric measurements, the curves were shifted according to the dependence of the transition temperature on the electric field and the pressure as reported in the literature.[6,7]

Author contributions

The manuscript was written through contributions from all authors. All authors have given approval to the final version of the manuscript.

Conflicts of interest

The authors declare no competing interests.

Data availability

CCDC 2039156–2039172 contain the supplementary crystallographic data for this paper.[62a–q]

The data supporting this article have been included as part of the supplementary information (SI). Supplementary information is available. See DOI: https://doi.org/10.1039/d6ta00623j.

The raw X-ray diffraction data (including integrated intensities and frame images) for all 17 temperatures reported in this study are openly available on Zenodo at https://zenodo.org/communities/thiourea. Each dataset is associated with a unique DOI, which is also linked to the corresponding CCDC deposition numbers (2039156–2039172).

Additional data will be available from authors upon reasonable request.

Acknowledgements

The authors acknowledge financial support from grant PID2021-122532OB-I00 funded by MCIU/AEI/10.13039/501100011033 and ERDF/EU and the projects ED431C 2022/39 and ED431F 2023/33 funded by Xunta de Galicia. This publication is part of the grant RYC2021-033040-I, funded by MCIU/AEI/10.13039/501100011033 and from the European Union ≪NextGenerationEU/PRTR≫. J. M. B.-G. is grateful for the support provided by the UDC-Inditex InTalent Programme. Funding for open access charge: Universidade da Coruña/CISUG.

References

1 F. Wöhler, *Ann. Phys.*, 1828, **88**, 253–256.
2 M. Nencki, *Ber. Dtsch. Chem. Ges.*, 1873, **6**, 598–600.
3 R. W. G. Wyckoff and R. B. Corey, *Z. Kristallogr. – Cryst. Mater.*, 1932, **81**, 386.
4 A. L. Solomon, *Phys. Rev.*, 1956, **104**, 1191.
5 G. J. Goldsmith and J. G. White, *J. Chem. Phys.*, 1959, **31**, 1175–1187.
6 H. Futama, *J. Phys. Soc. Jpn.*, 1962, **17**, 434–441.
7 K. Gesi, *J. Phys. Soc. Jpn.*, 1969, **26**, 107–112.
8 Y. Shiozaki, *Ferroelectrics*, 1971, **2**, 245–260.
9 D. R. McKenzie and J. S. Dryden, *J. Phys. C: Solid State Phys.*, 1973, **6**, 767–773.
10 A. H. Moudden, F. Denoyer, M. Lambert and W. Fitzgerald, *Solid State Commun.*, 1979, **32**, 933–936.
11 A. H. Moudden, D. E. Moncton and J. D. Axe, *Phys. Rev. Lett.*, 1983, **51**, 2390–2393.
12 C. P. Menon and J. Philip, *Ferroelectrics*, 2003, **287**, 63–70.
13 X. Moya, S. Kar-Narayan and N. D. Mathur, *Nat. Mater.*, 2014, **13**, 439–450.
14 E. Defay, R. Faye, G. Despesse, H. Strozyk, D. Sette, S. Crossley, X. Moya and N. D. Mathur, *Nat. Commun.*, 2018, **9**, 1827.
15 B. Nair, T. Usui, S. Crossley, S. Kurdi, G. G. Guzmán-Verri, X. Moya, S. Hirose and N. D. Mathur, *Nature*, 2019, **575**, 468–472.
16 A. Bergen, R. Andersen, M. Bauer, H. Boy, M. ter Brake, P. Brutsaert, C. Bührer, M. Dhallé, J. Hansen, H. ten Kate, J. Kellers, J. Krause, E. Krooshoop, C. Kruse, H. Kylling, M. Pilas, H. Pütz, A. Rebsdorf, M. Reckhard, E. Seitz, H. Springer, X. Song, N. Tzabar, S. Wessel, J. Wiezoreck, T. Winkler and K. Yagotyntsev, *Supercond. Sci. Technol.*, 2019, **32**, 125006.
17 W. Chen, M. DiPirro, I. McKinley, C. Cho and H. Tseng, *Cryogenics*, 2024, **141**, 103877.
18 A. Rai and S. A. Tassou, *Energy Convers. Manag.*, 2017, **150**, 914–923.
19 K. Klinar, J. Y. Law, V. Franco, X. Moya and A. Kitanovski, *Adv. Energy Mater.*, 2024, **14**, 2401739.
20 A. Barman, S. Kar-Narayan and D. Mukherjee, *Adv. Mater. Interfaces*, 2019, **6**, 1–31.
21 J. Shi, D. Han, Z. Li, L. Yang, S. G. Lu, Z. Zhong, J. Chen, Q. M. Zhang and X. Qian, *Joule*, 2019, **3**, 1200–1225.

22 X. Chen, W. Zhu and Q. M. Zhang, *iEnergy*, 2023, **2**, 100–108.
23 J. Mira, J. Rivas, L. E. Hueso, F. Rivadulla and M. A. López-Quintela, *J. Appl. Phys.*, 2002, **91**, 8903–8905.
24 J. Mira, F. Rivadulla, J. Rivas, A. Fondado, T. Guidi, R. Caciuffo, F. Carsughi, P. G. Radaelli and J. B. Goodenough, *Phys. Rev. Lett.*, 2003, **90**, 189901.
25 J. M. Bermúdez-García, M. Sánchez-Andújar, S. Castro-García, J. López-Beceiro, R. Artiaga and M. A. Señarís-Rodríguez, *Nat. Commun.*, 2017, **8**, 15715.
26 M. Gelpi, J. García-Ben, S. Rodríguez-Hermida, J. López-Beceiro, R. Artiaga, Á. Baaliña, M. Romero-Gómez, J. Romero-Gómez, S. Zaragoza, J. Salgado-Beceiro, J. Walker, C. J. McMonagle, S. Castro-García, M. Sánchez-Andújar, M. A. Señarís-Rodíguez and J. M. Bermúdez-García, *Adv. Mater.*, 2024, **36**, 2310499.
27 L. Abate, M. Jozwiak and G. Della Gatta, *Thermochim. Acta*, 1997, **303**, 63–68.
28 G. Della Gatta, M. Jóźwiak, B. Brunetti and L. Abate, *J. Chem. Thermodyn.*, 2000, **32**, 979–997.
29 S. Wang, Q. Gao and J. Wang, *J. Phys. Chem. B*, 2005, **109**, 17281–17289.
30 J. M. Igartua, A. LÓpez-Echarri, T. Breczewsk and I. Ruiz-Larrea, *Phase Transitions*, 1993, **46**, 47–55.
31 T. Hess, L. M. Maier, N. Bachmann, P. Corhan, O. Schäfer-Welsen, J. Wöllenstein and K. Bartholomé, *J. Appl. Phys.*, 2020, **127**, 075103.
32 P. F. Li, W. Q. Liao, Y. Y. Tang, H. Y. Ye, Y. Zhang and R. G. Xiong, *J. Am. Chem. Soc.*, 2017, **139**, 8752–8757.
33 X. Liu, Z. Wu, T. Guan, H. Jiang, P. Long, X. Li, C. Ji, S. Chen, Z. Sun and J. Luo, *Nat. Commun.*, 2021, **12**, 1–7.
34 S. Han, J. Bie, W. Fa, S. Chen, L. Tang, W. Guo, H. Xu, Y. Ma, Y. Liu, X. Liu, Z. Sun and J. Luo, *J. Am. Chem. Soc.*, 2024, **146**, 8298–8307.
35 J. J. Wang, D. Fortino, B. Wang, X. Zhao and L. Q. Chen, *Adv. Mater.*, 2020, **32**, 1–6.
36 H. B. von Bern, *Helv. Phys. Acta*, 1950, **Jg. 23**(6–7), 651–696.
37 X. Moya, E. Stern-Taulats, S. Crossley, D. González-Alonso, S. Kar-Narayan, A. Planes, L. Mañosa and N. D. Mathur, *Adv. Mater.*, 2013, **25**, 1360–1365.
38 G. Sebald, L. Seveyrat, D. Guyomar, L. Lebrun, B. Guiffard and S. Pruvost, *J. Appl. Phys.*, 2006, **100**, 124112.
39 B. A. Tuttle and D. A. Payne, *Ferroelectrics*, 1981, **37**, 603–606.
40 X. S. Qian, H. J. Ye, Y. T. Zhang, H. Gu, X. Li, C. A. Randall and Q. M. Zhang, *Adv. Funct. Mater.*, 2014, **24**, 1300–1305.
41 X. Li, X. Qian, S. G. Lu, J. Cheng, Z. Fang and Q. M. Zhang, *Appl. Phys. Lett.*, 2011, **99**, 052907.
42 Y. Sun, S. An, Y. Gao, Z. Yu, X. Yuan, Z. Ma, K. Shi, F. Hu and C. Wang, *J. Mater. Chem. A*, 2025, 6152–6175.
43 M. V. Gorev, E. A. Mikhaleva, I. N. Flerov and E. V. Bogdanov, *J. Alloys Compd.*, 2019, **806**, 1047–1051.
44 M. V. Gorev, E. V. Bogdanov and I. N. Flerov, *Scr. Mater.*, 2017, **139**, 53–57.
45 M. V. Gorev, E. V. Bogdanov and I. N. Flerov, *J. Phys. D Appl. Phys.*, 2017, **50**, 384002.
46 N. Saadatkhah, A. Carillo Garcia, S. Ackermann, P. Leclerc, M. Latifi, S. Samih, G. S. Patience and J. Chaouki, *Can. J. Chem. Eng.*, 2020, **98**, 34–43.
47 E. A. Mikhaleva, I. N. Flerov, V. S. Bondarev, M. V. Gorev, A. D. Vasiliev and T. N. Davydova, *Ferroelectrics*, 2012, **430**, 78–83.
48 V. S. Bondarev, E. A. Mikhaleva, M. V. Gorev and I. N. Flerov, *J. Alloys Compd.*, 2021, **892**, 162130.
49 V. S. Bondarev, E. A. Mikhaleva, M. V. Gorev and I. N. Flerov, *Solid State Commun.*, 2025, **395**, 115747.
50 Y. Lin, C. Chai, Z. Liu, J. Wang, S. Jin, Y. Yang, Y. Gao, M. Hao, X. Li, Y. Hou, X. Ma, B. Wang, Z. Wang, Y. Kan, J. Zheng, Y. Bai, Y. Chen, J. Sun, T. Zhao, J. Y. Law, V. Franco, F. Hu and B. Shen, *Nat. Commun.*, 2025, **16**, 4009.
51 D. R. McKenzie, *J. Phys. C Solid State Phys.*, 1975, **8**, 1607–1619.
52 A. Yamamoto, *Phys. Rev. B: Condens. Matter Mater. Phys.*, 1980, **22**, 373–379.
53 S. Tanisaki, H. Mashiyama and K. Hasebe, *Acta Crystallogr. Sect. B*, 1988, **44**, 441–445.
54 Y. Gao, M. Gajhede, P. Mallinson, V. Petricek and P. Coppens, *Phys. Rev. B: Condens. Matter Mater. Phys.*, 1988, **37**, 1825–1831.
55 Y. Gao and P. Coppens, *Acta Crystallogr. Sect. B*, 1989, **45**, 298–303.
56 I. Takahashi, A. Onodera and Y. Shiozaki, *Acta Crystallogr. Sect. B*, 1990, **46**, 661–664.
57 V. Petricek, P. Coppens and P. Becker, *Acta Crystallogr. Sect. A*, 1985, **41**, 478–483.
58 Bruker, *APEX3, Versión 2019.1-0*, Bruker AXS Inc.: Madison, Wisconsin, USA, 2019.
59 G. M. Sheldrick, *Acta Crystallogr. Sect. A Found. Crystallogr.*, 2015, **71**, 3–8.
60 G. M. Sheldrick, *Acta Crystallogr. C Struct. Chem.*, 2015, **71**, 3–8.
61 H. Kaddoussi, A. Lahmar, Y. Gagou, B. Asbani, G. Cordoyiannis, B. Allouche, H. Khemakhem, Z. Kutnjak and M. El Marssi, *J. Alloys Compd.*, 2016, **667**, 198–203.
62 (*a*) CCDC 2039156: Experimental Crystal Structure Determination, 2026, DOI: 10.5517/ccdc.csd.cc26fx7t.; (*b*) CCDC 2039157: Experimental Crystal Structure Determination, 2026, DOI: 10.5517/ccdc.csd.cc26fx8v; (*c*) CCDC 2039158: Experimental Crystal Structure Determination, 2026, DOI: 10.5517/ccdc.csd.cc26fx9w; (*d*) CCDC 2039159: Experimental Crystal Structure Determination, 2026, DOI: 10.5517/ccdc.csd.cc26fxbx; (*e*) CCDC 2039160: Experimental Crystal Structure Determination, 2026, DOI: 10.5517/ccdc.csd.cc26fxcy; (*f*) CCDC 2039161: Experimental Crystal Structure Determination, 2026, DOI: 10.5517/ccdc.csd.cc26fxdz; (*g*) CCDC 2039162: Experimental Crystal Structure Determination, 2026, DOI: 10.5517/ccdc.csd.cc26fxf0; (*h*) CCDC 2039163: Experimental Crystal Structure Determination, 2026, DOI: 10.5517/ccdc.csd.cc26fxg1; (*i*) CCDC 2039164: Experimental Crystal Structure Determination, 2026, DOI: 10.5517/ccdc.csd.cc26fxh2; (*j*) CCDC 2039165: Experimental Crystal Structure Determination, 2026, DOI: 10.5517/ccdc.csd.cc26fxj3; (*k*) CCDC 2039166: Experimental Crystal Structure Determination, 2026, DOI: 10.5517/ccdc.csd.cc26fxk4; (*l*)

CCDC 2039167: Experimental Crystal Structure Determination, 2026, DOI: 10.5517/ccdc.csd.cc26fxl5; (*m*) CCDC 2039168: Experimental Crystal Structure Determination, 2026, DOI: 10.5517/ccdc.csd.cc26fxm6; (*n*) CCDC 2039169: Experimental Crystal Structure Determination, 2026, DOI: 10.5517/ccdc.csd.cc26fxn7; (*o*) CCDC 2039170: Experimental Crystal Structure Determination, 2026, DOI: 10.5517/ccdc.csd.cc26fxp8; (*p*) CCDC 2039171: Experimental Crystal Structure Determination, 2026, DOI: 10.5517/ccdc.csd.cc26fxq9; (*q*) CCDC 2039172: Experimental Crystal Structure Determination, 2026, DOI: 10.5517/ccdc.csd.cc26fxrb.